ADVANCES IN TURBULENCE PHYSICS AND MODELING
BY DIRECT NUMERICAL SIMULATIONS

W. C. Reynolds

Department of Mechanical Engineering

Stanford University, Stanford, CA 94305-3030

1. Introduction

The advent of direct numerical simulations of turbulence has opened new avenues for research on turbulence physics and turbulence modeling. Although limited to relatively low Reynolds numbers, direct simulations have already provided new insight into the structure of turbulence. Direct numerical simulation provides values for anything that the scientist or modeler would like to know about the flow, and this is beginning to have tremendous payoff. Simulations have enabled detailed evaluations to be made of turbulence models intended for use in engineering codes, as well as models of the small-scale turbulence required for Large Eddy Simulations (LES), a promising technique for practical numerical simulations of turbulence at high Reynolds numbers. This paper presents an overview of some recent advances in the physical unsderstanding of turbulence and in turbulence modeling obtained through such simulations.

One class of turbulence that has been studied extensively by direct simulations is *homogeneous turbulence*. In homogeneous turbulence, the mean velocity gradients are prescribed and must be uniform in space, and all turbulence statistics are independent of position. One of the difficult problems in turbulence simulations is the provision of boundary conditions. It has been demonstrated that, in simulating homogeneous flows, one may use periodic boundary conditions, provided that the computational domain is larger than twice the distance between points where statistical motions are significantly correlated. Hence, the boundary motions do not have to be known to simulate homogeneous turbulence, but instead emerge as a result of the dynamics of the flow and the periodicity. It is for this reason that much of the first work on direct simulations has dealt with homogeneous turbulence.

A program developed by Dr. Robert Rogallo (1981) at Ames has become the bulwark of direct simulations of various homogeneous turbulent flows. The program uses de-aliased spectral methods to obtain high accuracy at small scales. It works in a coordinate system that deforms with the mean flow using variables that are computed exactly in the limit of very rapid distortions, and so the program has been used to cover a wide range of mean deformation conditions. The Rogallo code has been used to study the decay of isotropic turbulence, the response of isotropic turbulence to imposed mean strain and rotation, and homo-geneous shear flow, including scalar transport. This work spans the Ames supercomputers from ILLIAC-IV to CRAY-2, and has recently been adapted for use on Masscomp supermini computers.

This paper highlights the results of three recent Stanford Ph.D. Dissertations, carried out on the Cray-XMP at NASA/Ames under the direction of the author as part of a cooperative program of turbulence research with colleagues at Ames. This program, which has spanned well over a decade, has produced many of the currently active researchers in this field, and has been instrumental in the establishment of Ames as the world center for this type of research. A key outgrowth of this prorgam is the recently-formed *NASA/Stanford Center for Turbulence Research*, which will bring together experimentalists, computational scientists, and modelers in a concerted attack on the physics and modeling of turbulence.

Two of the disserations discussed below deal with homogeneous turbulence, and were carried out using the Rogallo code. They represent the current state-of-the art in simulations of such flows, and illustrate the sort of insight into turbulence physics and models that can be obtained from direct simulations. The third dissertation was the first direct simulation of the spatially-developing turbulent mixing layer, and is characteristic of the state of affairs in the direct simulation of flows of practical interest. Current work in extending this simulation to the supersonic mixing layer, for applications in both aerodynamics and scramjet engines, will be mentioned.

2. Response of turbulence to irrotational strain

Two of the building-block flows for turbulence modelers are (1) homogeneous turbulence undergoing incompressible, irrotational mean strain and (2) relaxation to isotropy after cessation of the mean straining. These two situations apply approximately to the turbulence (1) in the contraction section of low-speed wind tunnels and (2) in the straight test section following the nozzle. Hence, this idealized case has practical importance, especially in wind tunnels designed for low free-stream turbulence.

Different types of mean deformation are of interest. Wind tunnels are either axisymmetric or two-dimensional, and the behavior of the turbulence is quite different in these cases. A simple model based on the idea that the turbulence consists of a complex tangle of vortex filaments is useful in understanding these

differences. The streamwise strain stretches the vortex filaments that form the turbulence, concentrating the vorticity and increasing the intensity of the swirling motion around each filament. The cross-stream contraction pushes these filaments closer together. In axisymmetric contraction the filaments are pushed together from both sides, whereas in plane strain (e.g. two-dimensional mean contraction), the vortex filaments are pushed together only in one direction.

In the diffuser segment of a wind tunnel, a still different type of mean deformation is imposed. In a round diffuser, vortex filaments are stretched in the two cross-stream directions, and compressed in the streamwise direction. This deforms the filaments into thin sheets, giving rise to intense local shear layers in the flow.

This line of thinking suggests that the small-scale structure of the turbulence, as determined by the tangle of vortex filaments, should be different under different mean distortions. But one of the common premises in turbulence modeling is that the small-scale structure is isotropic, which is not consistent with the model of distorted filaments. The model also suggests that the rate of return to isotropy upon cessation of mean deformation should depend on the nature of the vortex filament tangle, i.e. on the nature of the prior mean strain. These are features that one would expect to see in a numerical simulation and would like to see exhibited by analyticals model of turbulence.

Moon Lee (1986), now a Postdoctoral Researcher at NASA/Ames, performed an extensive series of direct simulations of homogeneous turbulence subjected to a variety of irrotational strains, and also studied the relaxation upon cessation of mean deformation. The objective of his dissertation was to use the simulation data to evaluate second-order closure models of turbulence. His simulations used a 128^3 mesh, a second-order Runga-Kutta time advance, carefully-configured initial conditions, and were executed at Reynolds numbers, based on the length and velocity scales of the energy-containing motions, of the order of 50. Some background necessary for understanding the impact of his work will now be outlined.

In second-order closures, one deals with the Reynolds stress tensor

$$R_{ij} = \overline{u'_i u'_j} \qquad (1)$$

or, alternatively, with the turbulent velocity scale

$$q^2 = R_{ii} \qquad (2a)$$

and the *Reynolds stress anisotropy tensor*

$$b_{ij} = (R_{ij} - \frac{1}{3} q^2 \delta_{ij})/q^2. \qquad (2b)$$

In isotropic turbulence $b_{ij} = 0$. If the energy in one component, say u'_1, goes to zero, then $b_{11} = -\frac{1}{3}$; and

if all of the fluctuation energy is in one component, say u'_1, then $b_{11} = \frac{2}{3}$. Thus, the values of b_{ij} are limited. These limits are conveniently described in terms of the invariants of the b_{ij} tensor. The first invariant is $I_b = b_{ii} = 0$. The second and third invariants are

$$II_b = -\frac{1}{2} b_{ij} b_{ji} \qquad (3a)$$

and

$$III_b = \frac{1}{3} b_{ij} b_{jk} b_{ki}. \qquad (3b)$$

The limits outlined above translate into limits on II_b and III_b, and one finds that all possible states of turbulence must lie within a certain area on the III_b - II_b plane, which is called the *anisotropy invariant map* (AIM) for the Reynolds stress. Simple eddy viscosity models for the Reynolds stresses do not necesarily satisfy this condition, particularly in cases of very strong strain-rate, and hence sometimes these models produce *unrealizable turbulence*. The AIM is therefore a very useful tool for assessing turbulence models.

Second-order closure models for homogeneous flows require closures for the equations of evolution of R_{ij} and ϵ , the rate of dissipation of mechanical energy per unit volume by the turbulence. Alternatively, the evolution equations for b_{ij} and q^2 are used in place of those for R_{ij}. The turbulent kinetic energy equation describes the evolution of q^2, and is

$$\frac{dq^2}{dt} = 2(P - \epsilon) \qquad (4a)$$

where

$$P = -R_{ij} S_{ij} \qquad (4b)$$

is the rate of energy transfer from the mean motion to the turbulence (*production*) and

$$S_{ij} = \frac{1}{2}(U_{i,j} + U_{j,i}) \qquad (4c)$$

is the mean strain-rate (commas denote partial differentiation). No modeling is necessary in (4a) because it contains only the model variables and the prescribed mean velocity gradients.

The equation for b_{ij} is

$$\frac{db_{ij}}{dt} = A_{ij} - \frac{\epsilon}{q^2}(\phi_{ij} - 2b_{ij}). \qquad (5)$$

Here A_{ij} is a production term involving only the anisotropy tensor b and the mean velocity gradients, and hence does not require modeling. ϕ_{ij}, which involves the anisotropy of the viscous dissipation and the pressure-strain terms, must be modeled. It contains a *rapid pressure-strain* part that changes instantly when the mean velocity gradients are changed, which must be modeled as being proportional to the mean gradients, and *slow* terms that do not contain the mean

202

velocity gradients. For the special case of no mean gradients (the *return to isotropy* problem), ϕ_{ij} contains only the slow terms. Hence, the modeling of these terms can be examined by studying direct simulations of the return to isotropy, and this was the primary objective of Moon Lee's dissertation.

If one is going to work with b_{ij}, q^2, and ϵ as variables, then the model for ϕ_{ij} must be expressed interms of these variables. The tensor character must be carried by tensors developed from b_{ij}. By the Cayley-Hamilton theorem, there are only two linearly independent tensors that can be involved. Thus, the most general model of the slow part of ϕ_{ij} possible in this type of second-order closure is

$$\phi_{ij} = (\alpha + 2)b_{ij} + \beta\left(b_{ik}b_{kj} + \frac{2}{3}II_b\delta_{ij}\right) \qquad (6)$$

where α and β are scalar coefficients that can depend upon the scalar invariants II_b and III_b and on other scalars, such as the turbulent Reynolds number $R_T = q^4/(\epsilon\nu)$. An immediate consequence of this model is that the return to isotropy must follow a trajectory on the Reynolds stress AIM given by

$$\frac{dIII_b}{dII_b} = \frac{3\alpha III_b + \frac{2}{3}\beta II_b^2}{2\alpha II_b - 3\beta III_b}. \qquad (7)$$

Hence, the trajectory should be a unique function of the position on the AIM (and R_T). Thus, by following the trajectory in the simulations, one should be able to deduce the parameters α and β, *provided* that the assumed model is adequate to describe the flow.

The simulations showed that the return trajectory is *not* a unique function of the AIM state; the most striking deviations were in the case of axisymmetric expansion flows, where turbulence that had been rapidly strained actually moved further *away* from isotropy when the strain-rates was removed, while turbulence that had been strained slowly to the same anisotropy moved *towards* isotropy upon the removal. Thus, at least for the case of strong strain-rate (but of the order of the strain rate in many practical situations), the standard second-order model simply is inadequate.

We then turned to looking for alternative ways to characterize and model the turbulence, using two other tensors characterizing the anisotropy of the small-scale motions. Analogous to R_{ij}, q^2 and b_{ij} we define the vorticity tensor by

$$V_{ij} = \overline{\omega_i'\omega_j'} \qquad (8a)$$

where ω_i' is a turbulent vorticity component. The mean-square vorticity is

$$\omega^2 = V_{ii} \qquad (8b)$$

which, for homogeneous turbulence, is related to the dissipation by

$$\epsilon = \nu\omega^2. \qquad (8c)$$

The *vorticity anisotropy tensor* is defined by

$$v_{ij} = \frac{V_{ij} - \frac{1}{3}\omega^2\delta_{ij}}{\omega^2} \qquad (8d)$$

and its invariants, II_v and III_v are defined in the same way as those for **b**.

The dissipation is

$$D_{ij} = 2\nu\overline{u_{i,k}'u_{j,k}'}. \qquad (9a)$$

The trace of this tensor is

$$D_{ii} = 2\epsilon \qquad (9b)$$

The associated *dissipation anisotropy tensor* is defined by

$$d_{ij} = \frac{D_{ij} - \frac{2}{3}\epsilon\delta_{ij}}{2\epsilon} \qquad (9c)$$

and its invariants, II_d and III_d are defined in the same way as those for **b**.

The AIMs for **v** and **d** look exactly like that for **b**, although the phisical meanings of the limiting boundaries are different. For example, turbulence in which the vortex filaments have been stretched infinitely in one direction has a *one*-dimensional vorticity field but a *two*-dimensional velocity field, and hence its state is at different points on the **v** and **b** AIMs.

The simulations revealed a very surprising result that shakes the roots of turbulence theory. The anisotropy of the small-scale turbulence was *not* found to be much smaller than the anisotropy of the large-scale turbulence, as the lore of turbulence suggests. Instead, there tended to be strong relatonships between the anisotropies at small and larges scales, as revealed by the instantaneous states of the turbulence on the vorticity/dissipation AIMS and the Reynolds stress AIM, respectively. It has been suggested that this is a result of the low Reynolds numbers used in the simulations. However, we can see no trend for the small-scale anisotropy to be less at higher Reynolds numbers. Figure 1 shows the second invariants of the vorticity and Reynolds stress anisotropies during the relaxation from simple strains. Note that for virtually every field examined the vorticity anisotropy was larger than the Reynolds stress anisotropy, as measured by their second invariants. Figure 2 shows the dissipation anisotropy vs. that for the Reynolds stress for these same velocity fields. Note that the second invariants of these anisotropies are generally of comparable value, again indicating the non-isotropic nature of the small-scale field.

Upon further reflection on this problem, it is clear from the Biot-Savart law, which relates the velocity field to the vorticity field, that anisotropy in the Reynolds stress can only arise if there is anisotropy in the two-point vorticity correlation tensor. Since

the anisotropy in Reynolds stresses persists at high Reynolds numbers, the vorticity field must also exhibit important anisotropy at high Reynolds numbers. The simulations led us to focus on this issue, and they suggest that modeling of the large-scale turbulence might be improved by explicit consideration of the anisotropies of the vorticity.

Using the simulated fields as "data", we explored a number of possible models for the return to isotropy problem, seeking a model that would describe the evolution more accurately. We found that the return-to-isotropy trajectories on the vorticity and dissipation AIM's *were* unique, and hence the evolution equations for v_{ij} and d_{ij} can be closed by simple models in terms of their own tensors. For example, the vorticity anisotropy was found to obey (during return to isotropy)

$$\frac{dv_{ij}}{dt} = -\gamma \frac{\epsilon}{q^2} v_{ij} \qquad (10)$$

Lee was able to obtain a tidy formula describing the coefficient γ as a function of the invariants II_b and II_v, and had similar success with the dissipation anisotropy model. Figures 3 and 4 show the comparisons of his model trajectories on the vorticity and dissipation AIMs for the return-to-isotropy cases. But unfortunately a truly satisfactory model for the evolution of b_{ij} was not discovered, and so a complete second-order turbulence model has not yet been established.

In summary, Lee's simulations of homogeneous turbulence under irrotational strain provide some very important new insight into the physics of turbulence. They raise serious questions about traditional ideas of small-scale anisotropy that have been deeply imbedded in turbulence theory and modeling, and suggest that considertation of small-scale anisotropy may be essential for development of better turbulence models for the large-scale turbulence. Lee's velocity fields have been archived at Ames and are being used to study other aspects of turbulence physics and modeling. We expect that much more can be learned from them about turbulence.

3. Scalar transport in homogeneous shear flow

Homogeneous turbulent shear flow occurs when the mean velocity gradient transverse to the flow is uniform. This situation has been studied experimentally in special wind tunnels that use variable grids to establish this unusual mean flow, and has been explored in great depth using the Rogallo code.

In homogeneous turbulence there is no *net* gain or loss to an elemental control volume as a result of turbulent transport (the gradients of all turbulence correlations vanish in homogeneous turbulence). But the turbulent fluxes are still present, and they can be studied by direct simulation. Experiments on heat transfer in such a flow have been limited to cases with a mean temperature gradient aligned with the mean velocity

gradient and cross-stream to it. These experiments suggest that there are strong anisotropies in the turbulent diffusion of scalars (e.g. temperature or species) in shear flow, but not enough is known about these effects to allow them to be incorporated in turbulence models.

In an effort to shed more light on this problem, Mike Rogers (1986), now a Staff Scientist at Ames, carried out detailed simulations of homogeneous shear flow with various arrangements for scalar transport, using the Rogallo code. The flow considered had the mean shear rate

$$\frac{dU_1}{dx_2} = S \qquad (11)$$

and was examined with the three linearly-independent cases, each having a mean temperature gradient in only one direction, at Prandtl numbers of 1, 0.2, and 0.7, and covered a wide range of Sq^2/ϵ, the dimensionless shear rate parameter, and Reynolds numbers. Most were carried out with a 128^3 mesh, in some cases non-square. The computed velocity and scalar fields have been preserved at selected time intervals, and represent a great resource for subsequent study of new physical ideas or modeling concepts.

The case of primary interest is case 2, having a mean temperature gradient in the x_2 direction, for this is the usual alignment of the velocity gradient and temperature gradient in shear flows. The simulations confirm the rather surprising results of experiments that the heat flux in the direction *perpendicular* to the mean temperature gradient is significantly larger than the heat flux down the imposed mean temperature gradient! Hence, *simple* gradient-transport models that assume that the heat flux vector is aligned directly opposite to the mean temperature gradient will fail to predict the strong cross-gradient transport. There are many important practical situations where this coss-gradient transport is likely to be a very important phenomena, and so it is important that the mechanisms be understood and that the models be improved so that the fluxes can be predicted.

Rogers and Moin studied the structure of the turbulence field in shear flow in great detail, using the simulations to explore such questions as the configurations of vortex lines in the flow. They found that hairpin vorticies, of the type found in inhomogeneous shear flows over solid walls, also occur in homogeneous shear flow. These vortices arise as a result of the straining of vortex filaments, and the legs of the hairpin vortices are predominantly aligned with the axis of positive principal strain rate, i.e. at $45°$ upward from the x_1 axis. In homogeneous shear flows there are equal numbers of "heads-up" and "heads-down" hairpins. The vorticity in the heads has the same sense as the vorticity in the mean flow; indeed, much of the transverse vorticity is concentrated in these hairpin heads. Rogers also found that persistent shearing at

the higher Reynolds numbers gives rise to structures with strong spanwise coherence over substantial distances, very much like the two-dimensional rollers in a two-stream mixing layer. Thus, the dominant large-scale structures in homogeneous shear flow are now thought to be some combinations of spanwise vortices and up and down hairpins.

This model of the structure of the turbulence allows one to understand the anisotropic nature of the turbulent heat transport. Figure 5 shows Rogers' explanation of the way in which these three types of coherent structures act to convect the scalar field in each of the three cases.

Simple extensions of the gradient transport model can be used to predict the heat fluxes for arbitrary mean temperature gradients. In suggesting these models we are not proposing that the transport process is one of gradient diffusion at the molecular level, but only that the mean temperature gradient provides the *scaling* of the heat flux. The direction of the heat flux vector is determined in a complicated way by the fluid dynamics, but it turns out that it is possible to model this in either of two rather simple ways.

The first model uses an anisotropic tensor turbulent diffusivity D_{ij}, defined by

$$F_i = \overline{\theta' u_i'} = -D_{ij} \frac{\partial T}{\partial x_j} \qquad (12)$$

where θ' is the scalar(temperature) fluctuation, T is the mean scalar quantity (temperature), and F_i is the scalar flux in the ith direction. D_{ij} is easily calculated from the simulation data, and is found to be non-symmetric. However, in a rotated coordinate system it can be made antisymmetric, and the important thing discovered by Rogers is that this coordinate system is essentially the same as the principal coordinate system of R_{ij} and b_{ij}. This means that the diagonal members of D_{ij} should be modeled in terms of the Reynolds stress tensor. In the rotated coordinate system, the off-diagonal elements must be antisymmetric, and the only antisymmetric tensor available is the mean rotation tensor,

$$\Omega_{ij} = \frac{1}{2}(U_{i,j} - U_{j,i}). \qquad (13)$$

This leads one to the model

$$D_{ij} = \frac{q^4}{\epsilon}(C_1 b_{ij} + C_2 \delta_{ij} + C_3 \tau \Omega_{ij}) \qquad (14)$$

where τ is an appropriate turbulence time scale (q^2/ϵ) and the coefficients $C_1 - C_3$ are dimensionless functions of scalars in the model. Rogers fit the coefficients as functions of the Reynolds and Prandtl numbers, and found that the resulting model could predict all of the heat fluxes for all of his fields to within 20%. This

model can be used for inhomogeneous flows to estimate the anisotropic diffusivity tensor.

A second, more sophisticated model, containing only one free coefficient, was also evaluated by Rogers. This model assumes that certain vector terms needing to be modeled in the exact equation for the turbulent scalar flux are aligned with the flux vector. This assumption had been made intuitively by earlier modlers, but Rogers was able to check it in detail using the simulations, and found that it was indeed approximately true. This assumption allows the equation for the scalar flux to be reduced to

$$-R_{ij}\frac{\partial T}{\partial x_j} - F_j \frac{\partial U_i}{\partial x_j} + C\frac{F_i}{\tau} = 0. \qquad (15)$$

This is a set of linear algebraic equations for the F_i that can be inverted immediately for special gradients and solved locally in the general cases. Rogers fit the simulation results to determine C, and found that the resulting fluxes were predicted for all cases to within about 20%.

In summary, Rogers' simulations of scalar transport in homogeneous turbulent shear flow provide physical insight on the structure of homogeneous turbulent shear flow, an explanation for the mechanisms of cross-gradient turbulent heat transfer, and simple models that can be incorporated into codes for more complicated engineering problems. The fields have been archived at Ames and continue to be explored in the study of the physics and modeling of turbulence.

4. The spatially-developing mixing layer

The mixing layer between two parallel streams of different velocity has been widely studied in the laboratory and, for the case of *time-development*, by direct numerical simulation. The time-developing case has lent itself to simulation because it permits the use of periodic boundary conditions in the flow direction, thereby eliminating the need to devise turbulent inflow and outflow conditions.

In a dissertation just completed, Pat Lowery (1986), who did his research as a NASA CFD Fellow and now works in CFD at the Battelle Northwest Research Laboratories, developed a code for the spatially-developing mixing layer, including scalar transport, with prescribed time-dependent inlet conditions. He studied the *forced* mixing layer in a series of two- and three-dimensional simulations, which included mixing studies and a fast chemical reaction calculation.

Typical two-dimensional calculations used a mesh 256 (cross-stream) by 1024 (streamwise). Three-dimensional calculations used a mesh 512 (streamwise) by 128 (cross-stream) by 64 (spanwise). Finite-difference representations were used streamwise, spectral representations were used cross-stream and spanwise, and a third-order Runga-Kutta scheme was used for time advance. TVD corrections were necesary to maintain

205

proper scalar fields. On the Cray XMP 4-8, approximately 60 CPU seconds were required per time step in three-dimensions. The Reynolds number at the inlet to the computational domain, based on the velocity difference across the mixing layer and the inlet vorticity thickness, was 100; the Prandtl number was 1.

The first problem to be solved was the outflow boundary condition. Other workers have set gradients to zero at the outflow boundary, but this produces a "hard" exit condition that distorts the flow near the exit. Lowery found that a "softer" condition worked extremely well. The idea is simply to convect quantities out of the computational domain at a *uniform* convection velocity U_c by setting

$$\frac{\partial}{\partial t} + U_c \frac{\partial}{\partial x_1} = 0 \qquad (16)$$

for all of the velocity componts and the scalar field. This allows the large-scale structures to roll out of the computational domain at the convection velocity, which was taken as the average of the two free-stream speeds. Figure 6 shows a snapshot of Lowery's simulation, which strongly resembles pictures from experiments.

Most of the work was done with forcing at the inlet, which in Lowery's simulation was imagined to be just downstream of the splitter plate forming the mixing layer. Because the dynamical processes in the layer involve the interactions of modes with their subharmonics to produce vortex merging (the mechanism by which the turbulence scale grows larger downstream), it was necessary to excite the inlet flow with fundamentals and sub-harmonics of the basic instability modes for the inlet laminar shear layer (*tanh* profile). The response depends on the relative phases of these modes, and time permitted only a modest study of the possibilities. However, it became clear (as experiments have already shown) that control over the growth of the mixing layer can be achieved by careful selection of the subharmonic phases.

One of the major experimental observations is that more high-speed fluid is entrained into the layer than low-speed fluid. This effect is not captured in time-developing mixing layer simulations, since they are symmetric with respect to the two flow streams. This effect was captured in Lowery's simulations, at a level commensurate with experiments. Probability density functions, the turbulent stress behavior, and other features of the flows were comparable in trends and magnitudes with experimental forced mixing layers, although it was impossible to make a direct comparison because of the sensitivity to the particular forcing.

There are some theoretical arguments that suggest that the mixing layer is *convectively unstable*, meaning that removal of the forcing will permit the disturbances to wash downstream and the layer to re-laminarize. Lowery studied this question by freezing the disturbance field after some computation. Indeed, the disturbances washed downstream, but only partway. It seems that the large-scale disturbances in the far-downstream region trigger instabilities in the upstream flow through the pressure field. These new disturbances then travel downstream, repeating the triggering process (an *absolute instability*). It is generally believed that the splitter plate, absent in Lowery's simulation, is an essential element in making this flow absolutely unstable. The simulation suggests that this might not be the case.

In his three-dimensional simulations, Lowery added streamwise vortices to the forcing. These produced structures very similar to those seen in the "braid" regions of the mixing layer. He ran one simulation with random excitation at the inlet, and found that these same structures were beginning to emerge naturally, although a great deal more computational time would have to be expended to allow them to develop completely. Thus, one can probably study these three-dimensional effects by judicious selection of the inlet forcing.

Experiments have shown evidence of some vorticity of opposite sign to that in the mixing layer. This could be due to the vorticity coming from the boundary layer on the low-speed side of the splitter plate, or it could be due to overturning of vortex filaments by the three-dimensional action of the turbulence. Lowery could do what an experimentalist can not, i.e. run without the low-speed boundary layer, in which case negative vorticity could result only from overturning of vortex filaments. Feeding the inlet flow with vorticity of only one sign, only vorticity of this sign was found in the two-dimensional simulations. But in the three dimensional simulations a small amount of vorticity of opposite sign was found, indicating that the vortex filament overturning process indeed takes place.

A new Ph.D. student, Neil Sandham, has used Lowery's code to study the mixing layer using inlet flows representing the splitter-plate boundary layers. These have shown very little effect of the boundary layers on the overall flow development, except very near the end of the splitter plate. In addition, we have developed a method for randomly exciting the inlet flow that looks quite promising in that it produces a mixing layer behavior much more characteristic of natural mixing layers than of the forced layers studied by Lowery.

A new effort is being devoted to simulation of the *compressible* spatially-developing mixing layer, which is of interest in both aerodynamic and scramjet engine situations. The effort involves both direct numerical simulations at low Reynolds numbers and the development of improved models for LES studies of supersonic mixing and combustion. Supersonic mixing layers are known to spread and mix much less rapidly than subsonic layers, and the reasons for this are not well understood. In the scramjet application, new ways to

206

enhance the mixing must be found. We are hopeful that these direct simulations will, over the next few years, shed some light on these important questions.

In summary, Lowery's simulations of the spatially-developing mixing layer provide new physical insight into the mechanisms of transport and entrainment in inhomogeneous free shear flows, and provide a basis for further studies on the modeling of such flows. Inlet conditions for turbulent flows need to be developed, but the prospects look bright. Extensions to compressible flows are within reach and should be achieved in the next two or three years.

References

Lee, M.J. and W.C. Reynolds 1985 Numerical Experiments on the Structure of Homogeneous Turbulence, Report TF-24, Department of Mechanical Engineering, Stanford University

Lowery, P.S. and W.C. Reynolds 1986 Numerical Simulation of a Spatially-Developing, Forced, Plane Mixing Layer, Report TF-26, Department of Mechanical Engineering, Stanford University

Rogallo, R.S. 1981 Numerical Experiments in Homogeneous Turbulence. NASA Technical Memo 81315

Rogers, P.M, P. Moin and W.C. Reynolds 1986 The Structure and Modeling of the Hydrodynamics and Passive Scalar Fields in Homogeneous Turbulent Shear Flow, Report TF-25, Department of Mechanical Engineering, Stanford University
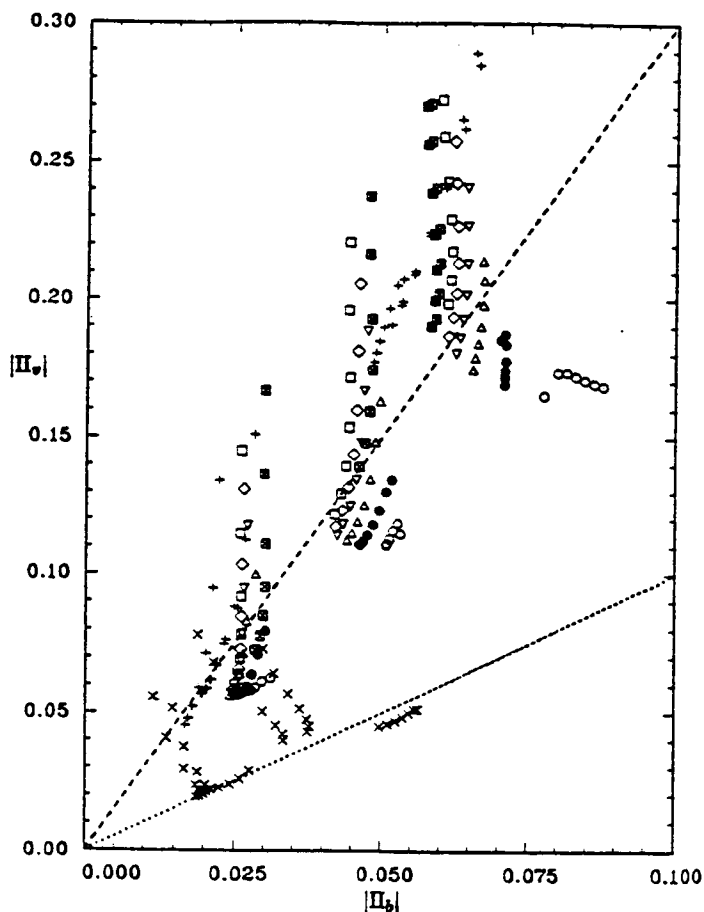
FIGURE 1

$|\mathrm{II}_v|$ vs. $|\mathrm{II}_b|$ for relaxation from simple strains. ●, AxR; △, BxR; ▽, CxR; ◇, DxR; □, ExR; ▣, FxR; ■, G1R; ⊙, HxR where $x =$ 2,3,4. +, relaxation from axisymmetric contraction; ×, relaxation from axisymmetric expansion. ----, locus of locking for relaxation from axisymmetric contraction ($A_b = -1$); ⸻, locus of locking for relaxation from axisymmetric expansion ($A_b = +1$).
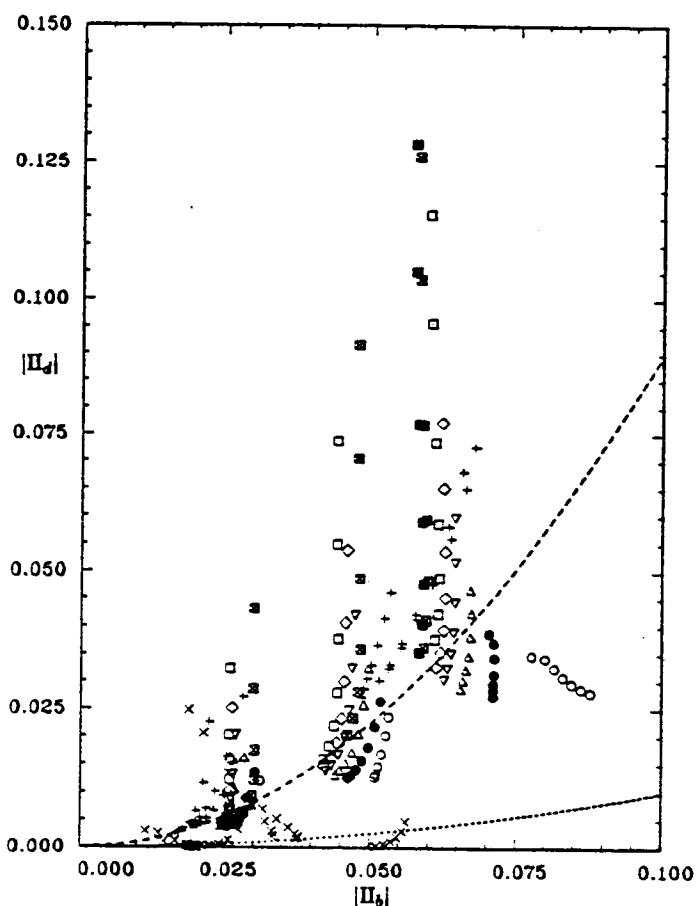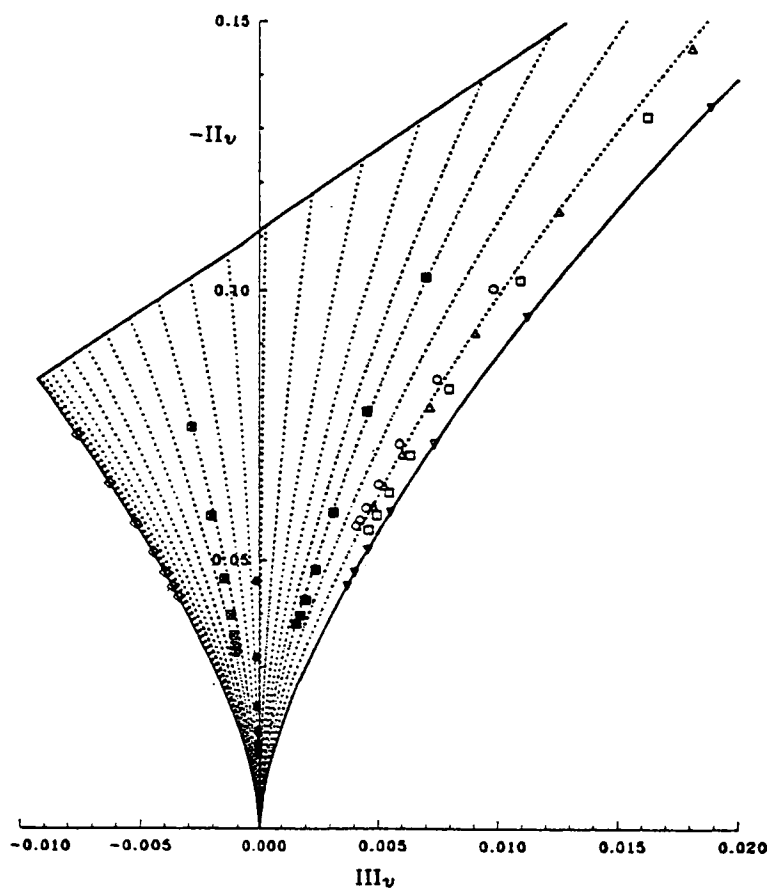

FIGURE 2

$|\mathrm{II}_d|$ vs. $|\mathrm{II}_b|$ for relaxation from simple strains. ●, AxR; △, BxR; ▽, CxR; ◇, DxR; □, ExR; ▣, FxR; ■, G1R; ⊙, HxR where $x =$ 2,3,4. +, relaxation from axisymmetric contraction; ×, relaxation from axisymmetric expansion. ----, locus of locking for relaxation from axisymmetric contraction ($A_b = -1$); ⸻, locus of locking for relaxation from axisymmetric expansion ($A_b = +1$).

FIGURE 3   Comparison of relaxation trajectories on the vorticity AIM: ⊙ , B2R;
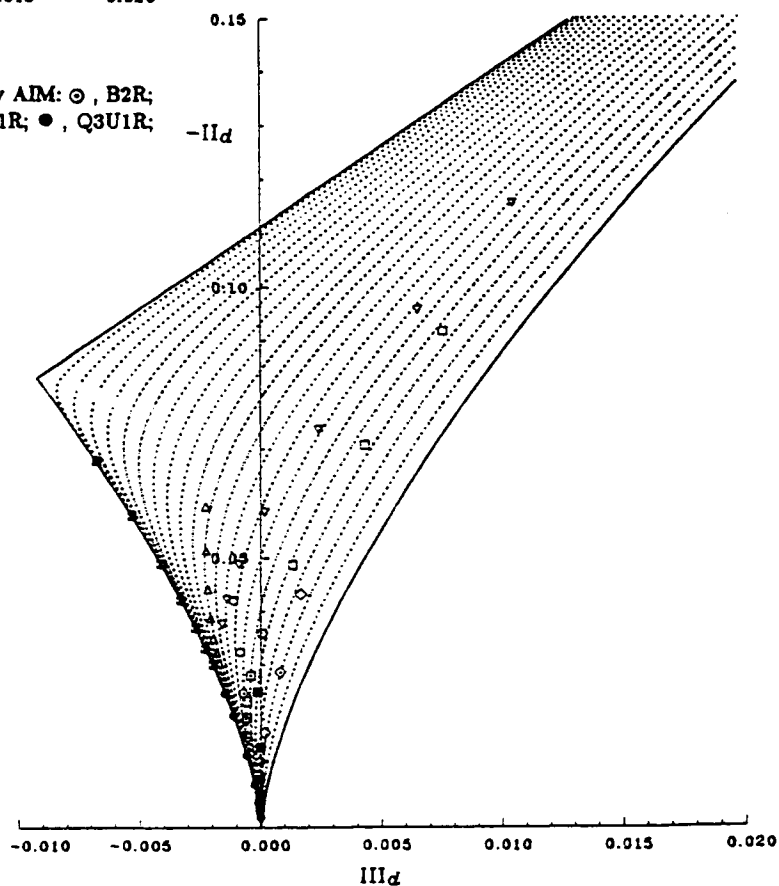△ , E2R; ▽ , M2R; ◇ , P6R; □ , L3W1R; ▣ , P3V1R; ● , Q3U1R;
■ , Q3W1R; ········ , model prediction.

FIGURE 4   Comparison of relaxation trajectories on the dissipation rate AIM: ⊙ ,
C3R; △ , C4R; ▽ , E4R; ◇ , F2R; □ , F3R; ▣ , L6R; ● , Q6R; ■ ,
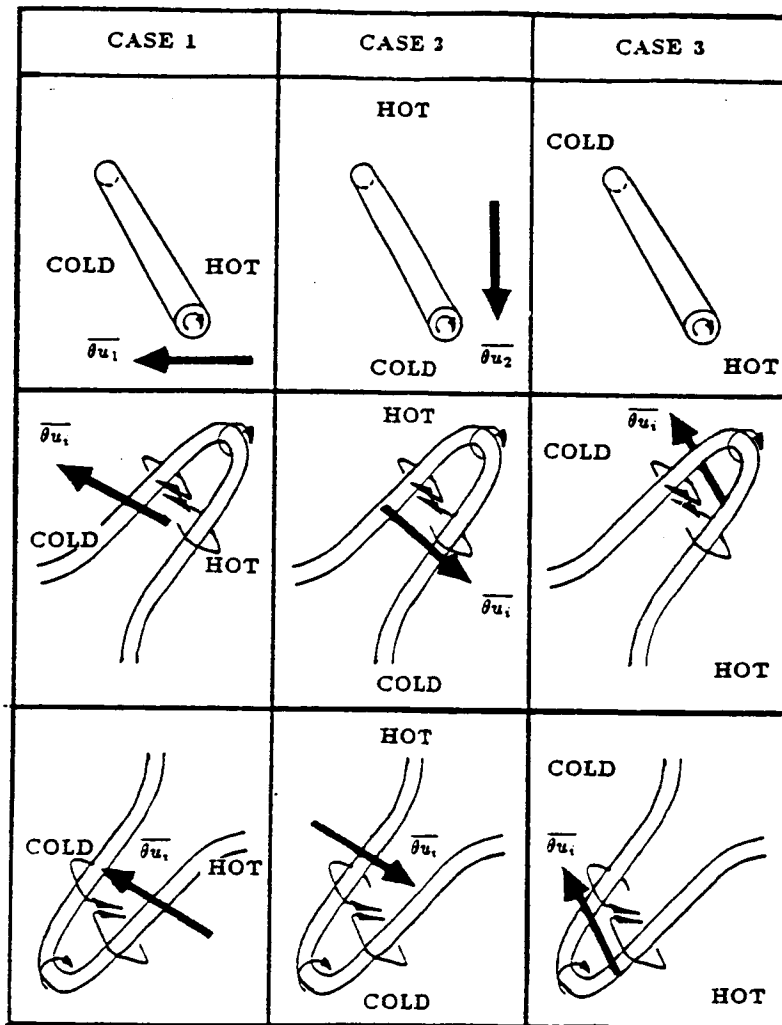L3W1R; ········ , model prediction.

Figure 5   Schematic of the turbulent scalar flux generated by typical coherent
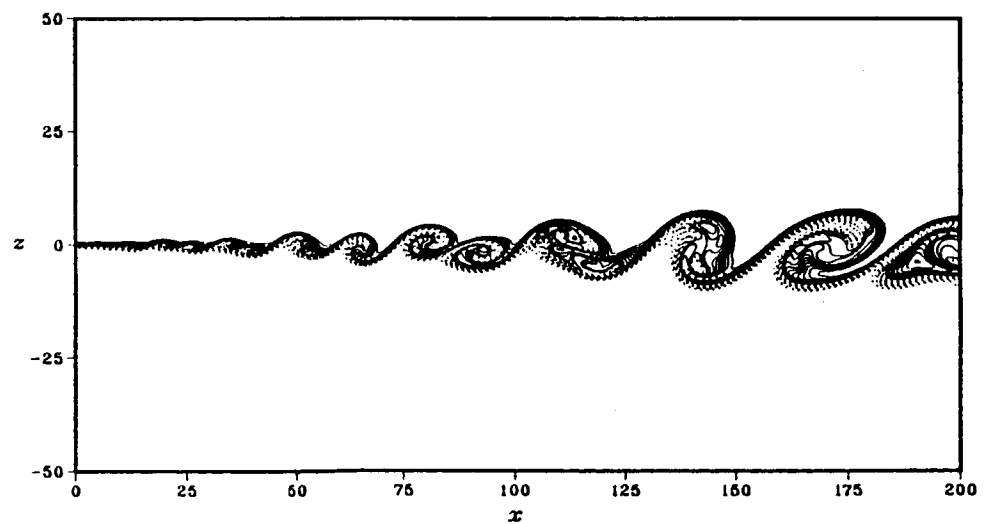structures for all three mean scalar gradient cases.

Figure   6   Snapshot" of results – passive scalar isograms

209